3D inversion of frequency-domain AEM surveys with a moving footprint

Leif H. Cox, Montana Tech and TechnoImaging, Glenn A. Wilson, TechnoImaging, and Michael S. Zhdanov, The University of Utah and TechnoImaging*

Summary

We show that it is practical to invert entire airborne electromagnetic (AEM) surveys to 3D conductivity models with hundreds of thousands of cells within a day on a workstation. We have exploited the fact that the area of the footprint of an AEM system is significantly smaller than the area of an AEM survey to develop a robust 3D inversion method which uses a moving footprint. Our implementation is based on the 3D integral equation method for computing AEM data and sensitivities, and the re-weighted regularized conjugate gradient method is used to minimize the objective functional. Even for terranes which are arguably as close to 1D as geologically possible, we demonstrate that results from our 3D inversion are a significant improvement over those models obtained from layered earth inversion. We demonstrate this with 3D inversion of RESOLVE frequency-domain AEM data acquired for salinity mapping over the Bookpurnong Irrigation District in South Australia.

Introduction

Airborne electromagnetic (AEM) data are often interpreted using conductivity depth transforms, layered earth inversions or laterally constrained layered earth inversions. Despite the widespread use of these 1D methods, it has been demonstrated that they are invalid for recovering models for simple 2D and 3D targets, let alone anything reflecting geological complexity. Despite this, the volume of data acquired in a typical AEM survey is so large that the various 1D methods are considered the only practical approach to interpretation. The problem with 3D modeling is that it is non-trivial given the necessity to solve as many large linear systems of equations as there are transmitter positions in the survey. For 3D inversion, this problem is exacerbated as sensitivities also need to be computed using adjoint operators, and the whole process has to be repeated for multiple iterations. Besides computational issues, the major limitation of 3D inversion is limited memory for storing the large but sparse sensitivity matrix. The sparseness of the sensitivity matrix is due to the relatively limited footprint of the AEM system. As an example, for frequency-domain AEM systems, Liu and Becker (1990) stated that at the inductive limit, the footprints for the horizontal coplanar and vertical coaxial components are 3.75*h* and 1.35*h*, respectively, where *h* is the flight height of the transmitter. Reid et al. (2006) showed that the footprints may be as high as 10 times the flight height for low induction numbers.

For frequency-domain AEM systems, the footprint maybe less than 400 m. The area is much smaller than the area of an AEM survey. The use of a moving footprint allows for the modeling and inversion of those parts of the model within the footprint of a particular transmitter-receiver pair rather than the entire AEM survey. In a practical context, this is equivalent to setting all irrelevant sensitivities to zero. The sensitivity matrix is constructed and stored as a sparse matrix for use in a regularized reweighted conjugate gradient method (Zhdanov, 2002, 2009) since the footprints of all the transmitter-receiver pairs superimpose themselves over the same 3D model. This makes it practical to invert tens of thousands of stations of AEM data to models with hundreds of thousands of cells within a day on a workstation. Cox and Zhdanov (2007) used a similar footprint approach for frequency-domain AEM where their 3D modeling and inversion was based on a combination of the localized quasi-linear (LQL) and full integral equation methods. In our implementation, there are no approximations in the modeling or inversion kernels. We demonstrate our approach with 3D inversion of an entire RESOLVE survey acquired for salinity mapping over the Bookpurnong Irrigation District in South Australia.

Inversion methodology

Conjugate gradient methods are the only practical approach to solving large-scale 3D inversion problems as they update the model conductivities with an iterative scheme akin to:

$$\boldsymbol{\sigma}_{i+1} = \boldsymbol{\sigma}_i + \Delta\boldsymbol{\sigma}_i = \boldsymbol{\sigma}_i + k_i \mathbf{F}_i^* \mathbf{r}_i, \qquad (1)$$

where k_i is a step length, $\mathbf{F}_i^*$ is the generalized inverse of the $N_d \times N_m$ Fréchet matrix $\mathbf{F}_i$ of normalized sensitivities, and $\mathbf{r}_i$ is the N_d length vector of the residual fields between the observed and predicted data on the i^{th} iteration. The iterative scheme consists of matrix-vector multiplications rather than pseudo-inverse matrix operations per Gauss-Newton methods. Data and model weights which re-weigh the inverse problem in logarithmic space are introduced in order to reduce the dynamic range of both the data and conductivity. The inversion iterates until the residual error reaches a pre-set threshold, the decrease in error between multiple iterations becomes less than a pre-set threshold, or a maximum number of iterations is reached. Given the limited footprint of the AEM system, not every transmitter has sensitivity to every cell.

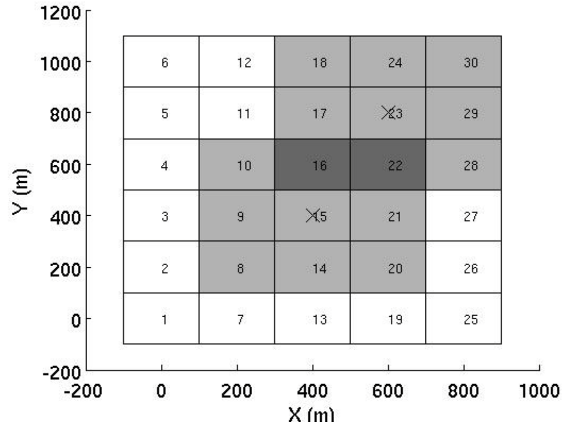

Figure 1. *Example inversion domain. The cells are numbered for clarity and correspond to the text. Two transmitter positions are centred upon cells 15 and 23; referred to as 1 and 2, respectively. The original inversion domain is the entire domain. The shaded cells around each transmitter map the footprint of the AEM system. The darker shaded cells from the overlap of the footprints are common to both footprints.*

In a moving footprint inversion, each transmitter-receiver pair is assumed only to contain sensitivity to those cells within its footprint. This means we exclude those cells outside the footprint by simply excluding them from the summation. This is equivalent to setting all irrelevant sensitivities to zero. As these values don't contribute to inversion, there is no need to compute nor to include them in modeling. Referring to Figure 1, we now only include those cells in the shaded region for each transmitter. To accomplish this, equation (1) is modified to, for example:

$$\Delta\sigma_{i,j} = k_i \sum F^*_{n,j} r_n, \qquad (2)$$

where:

$$n = \begin{cases} 1 & \text{if } j = 8, 9, 10, 14, 15, 20, 21, \\ 2 & \text{if } j = 17, 18, 23, 24, 28, 29, 30, \\ 1,2 & \text{if } j = 16, 22, \end{cases}$$

with the numbers given for j corresponding to the cells shown in Figure 1. There is no need to calculate the Green's body-to-receiver tensors and background fields for these cells. Moreover, since the background model is horizontally layered, the body-body Green's tensors are horizontally invariant. The electric Green's tensors are identical for each footprint domain and are then translated over the entire inversion domain, speeding up the computation and increasing memory efficiency.

Our 3D frequency-domain modeling is based on an implementation of the contraction integral equation method that exploits the Toeplitz structure of the large, dense matrix system in order to solve multiple right-hand side source vectors using an iterative method with fast matrix-vector multiplications provided by a 2D FFT convolution (Hursán and Zhdanov, 2002). This implementation reduces storage and complexity, and lends itself well to parallelization. Once the Green's tensors have been pre-computed, they are stored and re-used, further reducing runtime.

Case study - Bookpurnong

The Bookpurnong Irrigation District is located along the Murray River, approximately 12 km upstream from the township of Loxton, South Australia. This area has been the focus of various trials to manage a decline in vegetation; largely in response to floodplain salinisation from groundwater discharge in combination with decreased flooding frequency, permanent weir pool levels and recent drought. Various ground-based, river-borne and AEM methods have been deployed with the intent of mapping the distribution of salinity in the floodplain soils and groundwater. The intent is to indicate patterns and processes relating to groundwater evapotranspiration and flow across the salinising floodplains. We refer the readers to Munday et al. (2007) for a more detailed description of the geology, hydrology, and various river, borehole, ground and airborne electromagnetic surveys. We will constrain ourselves to a brief overview of the area, and will focus on the 3D inversion of that AEM data which has been the subject of previous 1D analysis (Viezolli et al., 2009).

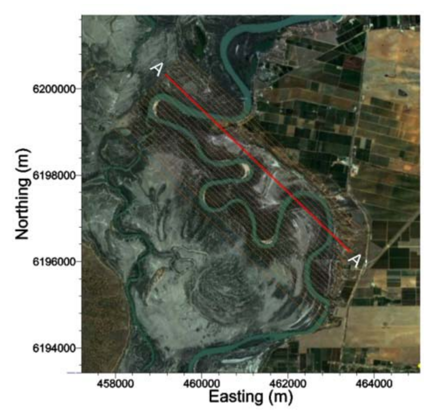

Figure 2. *Location map of the Bookpurnong Irrigation District, with RESOLVE (red) flight lines superimposed.*

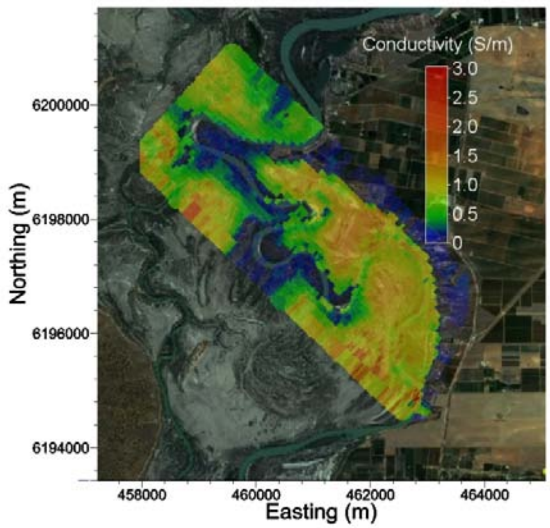

Figure 3. *Horizontal cross-section at 4 m depth of conductivity obtained from interpolation of layered earth inversions of the RESOLVE data using* AirBeo.

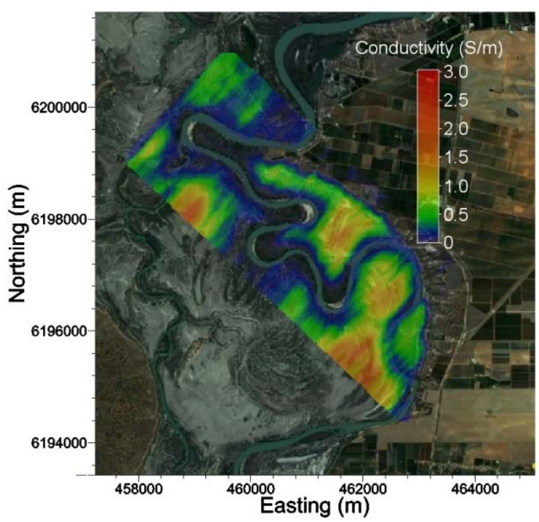

Figure 4. *Horizontal cross-section at 4 m depth of conductivity extracted from the 3D inversion of the RESOLVE data.*

The Bookpurnong area was flown with the RESOLVE frequency-domain helicopter system in both July 2005 and August 2008. We will concern ourselves with the August 2008 data. The RESOLVE system was configured with six operating frequencies: 390; 1798; 8177; 39,460; and 132,700 Hz horizontal coplanar and 3242 Hz vertical coaxial. The transmitter-receiver separation was 7.91 m for the five horizontal coplanar coil sets, and 8.99 m for the single vertical coaxial coil set. This 146 line km survey was flown as 26 lines oriented in a NW-SE direction with 100 m line spacing, and 7 tie lines (Figure 2). The survey was flown with a nominal bird height of approximately 45 m due to the presence of trees along the river bank.

The RESOLVE data were inverted for a 3D conductivity model with approximately 230,000 cells that were 25 m x 25 m in horizontal directions, and varied from 4.9 m to 25 m in the vertical direction. This grid was superimposed on a 20 Ωm half-space background conductivity model. The footprint of the RESOLVE system was set at 200 m. For comparison to 1D interpretation, we inverted all stations of the RESOLVE data for layered earth models using *AirBeo* (Raiche et al., 2007). The initial model for each station was a 20 ohm-m half-space containing four layers. The resistivity and thickness of each layer was allowed to vary.

The results obtained from the layered earth inversions are generally consistent with the laterally constrained inversions described by Munday et al. (2007) and Viezzoli et al. (2009). However, several notable features not clear in the various layered earth interpretations were clearly defined in the 3D inversion which was. Figure 3 shows a slice of the model at 4 m depth derived from interpolation of the layered earth inversion results for RESOLVE. Figure 4 shows the same slice at the same depth and same color scale but for the 3D inversion results. It is shown that 3D inversion of AEM data is practical. In the case study presented here, the 3D inversion of the RESOLVE data required 9 hours on a Windows workstation with a 2.4 GHz serial processor and 8 GB RAM. This compares well to the 3 hours needed for the 1D inversions computed on the same workstation.

Figure 5 compares two cross-sections from profile A-A`, shown in Figure 2. The thickness of the upper resistive layer is very similar between the two images. This corresponds to the depth to the water table which varies from 2 m to 6 m thick in this area (Munday et al., 2007). At depth, however, the 3D inversion creates a very coherent image of the losing and gaining sections of the river, while the layered earth inversion produces a section more difficult to interpret. The river channels on the right are clearly in a losing section, where the river flushes the surrounding area. The channels on the left are in a gaining section where the salinity is increased by the runoff from the irrigation district. The Murray River, which has a lower conductivity than the floodplains, is clearly visible in both 3D inversion results. The layered earth inversion smears the results, and in some areas, fails to show the presence of the Murray River. This is not just a limitation of layered earth inversion. Even laterally constrained inversions of the same area presented by Viezzoli et al. (2009) fail to detect the Murray River altogether.

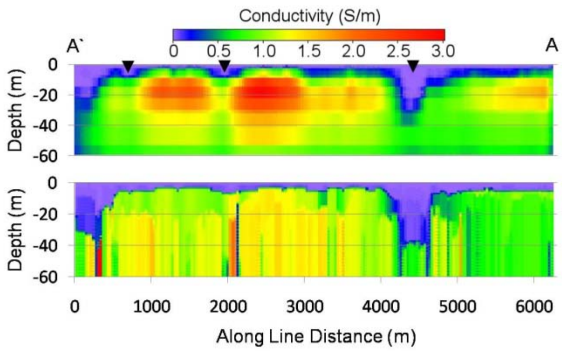

Figure 5. *2D vertical cross-section of conductivity along profile A-A' (shown in Figure 2) obtained from the 3D inversion of the RESOLVE data (top panel) and from the interpolation of layered earth inversions of the RESOLVE data using* AirBeo *(bottom panel). The locations where the river channel crosses the figure are shown by the black triangles. The channel on the right is in the losing section, and the two channels on the left are in a gaining section. A vertical exaggeration of 20 is applied to this image.*

Conclusions

3D inversion of entire AEM surveys is now a practical consideration, with runtimes less than a day for both frequency-domain AEM systems. We have exploited the fact that the area of an AEM system's footprint is much smaller than the area of an AEM survey. Our implementation naturally extends to time-domain AEM, and lends itself to parallelization. We are now in the process of distributing the software on massively parallelized architectures. This will further decrease the runtime, and will enable even larger surveys to be inverted (and interpreted) in 3D.

It is often argued that AEM for salinity mapping is ideally suited to various layered earth interpretation methods because of the high conductance of the ground, relative continuity of horizons, and their ability to interpret entire surveys rapidly. As we have demonstrated with our inversion of RESOLVE data, this is not necessarily true; especially as too much emphasis has been on inverting data rapidly without quality control on the models produced. Our case study has shown that 3D inversion results are in far better agreement with the known geology of the area than those results obtained from layered earth and laterally constrained inversions. Since layered earth inversion has been shown to fail in an area where a layered earth approximation would have been assumed adequate, one may wonder how erroneous layered earth interpretations may be in more complex terranes.

Acknowledgements

The Riverland AEM data presented in this paper were financed in part by the South Australian CNMR Board Project 054127: *The application of airborne geophysics to the prediction of groundwater recharge and floodplain salinity management*, and the CSIRO National Flagship program Water for a Healthy Country through the Regional Water theme. We acknowledge their permission to publish this work, and thank Dr. Andrew Fitzpatrick at CSIRO Earth Science and Resource Engineering for his assistance with regard to the Riverland AEM data. We also acknowledge TechnoImaging for permission to publish.

EDITED REFERENCES

Note: This reference list is a copy-edited version of the reference list submitted by the author. Reference lists for the 2010 SEG Technical Program Expanded Abstracts have been copy edited so that references provided with the online metadata for each paper will achieve a high degree of linking to cited sources that appear on the Web.

REFERENCES

Cox, L. H., and M. S. Zhdanov, 2007, Large scale 3D inversion of HEM data using a moving footprint: 77th Annual International Meeting, SEG, Expanded Abstracts, 467-470.

Hursán, G., and M. S. Zhdanov, 2002, Contraction integral equation method in three-dimensional electromagnetic modeling: Radio Science, **37**, no. 6, 1089, doi:10.1029/2001RS002513.

Liu, G., and A. Becker, 1990, Two-dimensional mapping of sea-ice keels with airborne electromagnetic: Geophysics, **55**, 239–248, doi:10.1190/1.1442832.

Munday, T., A. Fitzpatrick, J. Reid, V. Berens, and D. Sattel, 2007, Frequency and/or time-domain HEM systems for defining floodplain processes linked to the salinisation along the Murray River: Presented at 19th ASEG Geophysical Conference and Exhibition.

Raiche, A., F. Sugeng, and G. Wilson, 2007, Practical 3D EM inversion – P223F software suite: Presented at 19th ASEG Geophysical Conference and Exhibition.

Reid, J. E., A. Pfaffling, and J. Vrbancich, 2006, Airborne electromagnetic footprints in 1D earths: Geophysics, **71**, no. 2, G63–G72, doi:10.1190/1.2187756.

Viezzoli, A., E. Auken, and T. Munday, 2009, Spatially constrained inversion for quasi 3D modelling of airborne electromagnetic data – an application for environmental assessment in the Lower Murray Region of South Australia: Exploration Geophysics, **40**, no. 2, 173–183, doi:10.1071/EG08027.

Zhdanov, M. S., 2002, Geophysical Inverse Theory and Regularization Problems: Elsevier.

Zhdanov, M. S., 2009, Geophysical Electromagnetic Theory and Methods: Elsevier.